First-principles study of the lattice instabilities in Mn_2NiX (X= Al, Ga, In, Sn) magnetic shape memory alloys

Souvik Paul,[1] Biplab Sanyal,[2] and Subhradip Ghosh[1,*]

[1] *Department of Physics, Indian Institute of Technology Guwahati, Guwahati, Assam 781039, India*
[2] *Department of Physics and Astronomy, Uppsala University, Box 516, 75120 Uppsala, Sweden*

(Dated: March 1, 2024)

Using first-principles based Density Functional Theory (DFT), we have investigated the structural instabilities in the austenite phases of Mn_2NiX (X= Al, Ga, In, Sn) magnetic shape memory alloys (MSMA). A complete softening is observed in the acoustic TA_2 branches for all the materials along [$\xi\xi$0] directions leading to the instability in the austenite structure which effectively stabilizes into martensitic structure. The reasons behind this softening are traced back to the repulsion from the optical T_{2g} branches and to the nesting features in the Fermi surfaces. The vibrational density of states, the force constants and the elastic moduli are also computed and analyzed, which reconfirm the underlying mechanism behind the instabilities. The results indicate that the phonon anomalies are related to the occurrence of possible pre-martensitic phases which can be quite complex.

I. INTRODUCTION

Magnetic shape memory alloys (MSMA) are excellent candidates for technological applications due to their coupling between different degrees of freedom, such as caloric, magnetic, elastic etc., that introduce multifunctionality in these materials. The magneto-structural coupling results in a phase transition between high temperature austenite structure and low temperature martensitic variants driven by magnetic field under ambient conditions. Microscopically, this martensitic transformation is merely a consequence of reshuffling of atomic planes, which is often mediated through different periodically modulated meta-stable structures called premartensitic structure.

Very often, the microscopic origin behind the martensitic phase transformation can be explained by softening of some phonon modes, related to the softness in elastic stiffness constants caused by the nesting topology between parallel Fermi surfaces due to intense electron-phonon coupling.This has been the case for almost all the ternary MSMA's crystallizing in Heusler structure. The most extensively studied ternary MSMA is Ni_2MnGa, which in single crystal environments and close to the stoichiometric composition, exhibit nearly 10% magnetic field-induced strains (MFIS) under a magnetic field of less than 1 Tesla[1,2], making it a strong contender for micro-mechanical sensors and actuators. The structural instability of Ni_2MnGa in the austenite phase has been linked with an anomalous phonon softening of transverse acoustic TA_2 branch along [$\xi\xi$0] direction. The softening occurs at a fractional wave vector ξ=(0.33,0.33,0) and it becomes more prominent as one approaches towards the martensitic phase with decreasing temperature[3–6]. The phonon softening has been found to correlate with the premartensitic phase, which is anticipated by the precursor phonon softening at that wave vector. Inelastic neutron scattering experiments and elastic constants measurements on the high temperature phase corroborated the theoretical calculations of softening of acoustic branch. A complete softening of acoustic TA_2 branch along [$\xi\xi$0] direction with unstable phonon modes was reported theoretically in Ni_2MnAl[7]. Later, Moya *et al.* verified the Kohn anomaly observed in the theoretical study of TA_2 branch in this material by performing inelastic neutron scattering experiment on nearly stoichiometric Ni_2MnAl[8]. However, the experimental softening is not complete since the phonon frequencies remain finite even at lowest temperature. This could be related to the fact that the composition needed for the martensitic phase transformation to occur in Ni_2MnAl is slightly off-stoichiometric[9]. First-principles calculations observed similar phonon softening of the same acoustic branch in Ni_2MnIn, Ni_2MnSb, and Ni_2MnSn[10,11].

Although Ni_2MnGa near the stoichiometric composition is the first discovered ternary system in Heusler structure exhibiting magnetic shape memory effect, and has been studied extensively revealing a lot of interesting physics, its use in practical applications is hindered due to the martensitic transformation temperature being lower than the room temperature, and poor ductility in poly-crystalline phase[12,13]. Attempts were made to improve the functionality of the material by introducing disorder with various possibilities and replacing Ga conjointly with Al, Ge, In, Sn and Sb. However, the yield is not as fruitful as expected. Therefore, a quest for new MSMA began with higher operating temperatures and better elastic properties compared to Ni_2MnX. Recently, Mn_2NiGa has been reported to be a MSMA with promising functional properties[14–17]. It has a martensitic transformation temperature close to room temperature (270 K) and much broader hysteresis loop[14]. An excellent two-way shape memory effect with strains of 1.7% and field controllable shape memory effect up to 4% has been observed experimentally in single crystalline environment[14]. Experiments with poly-crystalline sample found the martensitic transformation temperature to be at 230 K[16]. It also observed that the structural transformation is dependent upon residual stress. According to the analysis of their Powder X-ray diffraction data,

the system undergoes a martensitic transformation to either a non-modulated tetragonal structure or a monoclinic modulated structure at room temperature, depending upon the residual stress. Neutron Powder diffraction experiments on this system confirmed the presence of an orthorhombic modulated structure, which is independent of temperature[17]. These results generated interests in this system in the context of understanding its structural stability and connections to shape memory effect. Another reason is that this material draws attention due to its relatively high Curie temperature ($T_C \sim 588$ K)[14] compared to Ni_2MnGa. In this respect, it is notable that Mn_2NiSn also has a high T_C (530 K)[18]. Driven by the possibilities of realizing new MSMAs with functionalities better than the Ni_2MnX ones, first-principles electronic structure calculations have been done on Mn_2NiX (X= Al, Ga, In, Sn) systems[19–23]. The results are quite encouraging as the total energy calculations predicted transformations from cubic austenite to a non-modulated tetragonal phase at low temperatures conserving the volume, a signature of shape-memory property. These results thus open up the possibility to further investigate the origin of such transformations and their consequences in these materials.

In this paper, we, therefore, make an attempt to understand the physical origin behind the transformations by examining the vibrational properties of these materials in a systematic way. We compute the phonon dispersion, the vibrational density of states, the elastic constants and the Fermi surfaces in order to see whether connections to the martensitic transformations can be made for these materials. The paper is organized as follows: in section II, we provide details of the computational methods used, in section III, we discuss the phonon dispersion relations, the vibrational densities of states, the inter-atomic force constants, the elastic constants and the Fermi surfaces in order to ascertain the mechanisms driving the martensitic transformations and finally we summarize our results indicating their relevance for future research.

II. COMPUTATIONAL DETAILS

The electronic structures of the systems considered were calculated using the Plane-Wave Pseudopotential (PW-PP) formalism of the Density Functional Theory (DFT), as implemented in Quantum Espresso[24] . UltraSoft Pseudo Potentials (USPP)[25] were used to accurately calculate the electronic ground states. Spin polarized Generalized Gradient Approximation (GGA) scheme was used as the exchange-correlation part of the potential with Perdew-Wang 91 parameterizations (PW91)[26]. Plane waves with energies up to 544 eV were used to describe electronic wave functions. Fourier component of the augmented charge density with cut-off energy up to 6530 eV was taken after convergence tests. The Brillouin zone integrations were carried out with finite temperature Methfessel-Paxton smearing[27] method using 12×12×12 uniform k-mesh, which effectively leads to 364 k-points in the irreducible wedge of the Brillouin zone. The value of the smearing parameter was taken as 0.27 eV. Such choices of the parameters ensure the convergence of phonon frequencies within 5%.

The phonon dispersion relations were computed using Density Functional Perturbation Theory (DFPT)[28]. The DFPT scheme is employed to accurately calculate the dynamical properties in condensed matter systems with the precision at par with the electronic structure calculations. The energy threshold value for convergence was 10^{-16} Ry in phonon calculations. Dynamical matrices were conveniently calculated in reciprocal space from the ground state charge density and from its linear response to the distortion in the ionic configurations. Fourier transform was employed thereafter to obtain the real space force constants. The dynamical matrices were calculated in a 4×4×4 q-point grid for all the structures. Convergence of phonon frequencies within $1-2\%$ was ensured by comparing frequencies calculated directly and frequencies obtained by the Fourier transform of the dynamical matrices. Such convergence tests ensured accuracy in elastic constants as they are calculated from the slopes of the phonon dispersion curves. The Fermi surfaces were calculated on $24 \times 24 \times 24$ highly dense uniform k-point grid. It may be noted that the strength of the phonon anomaly is extremely sensitive to temperature. An increase in temperature can reduce the nesting features of Fermi surfaces and thus weaken the anomaly. In DFT based calculations, the smearing parameter σ plays the role of fictitious electronic temperature. Therefore, to reduce the effect of finite temperature in the calculations of Fermi surfaces, we kept σ=0.01 eV all along.

III. RESULTS AND DISCUSSIONS

A. Phonon dispersion

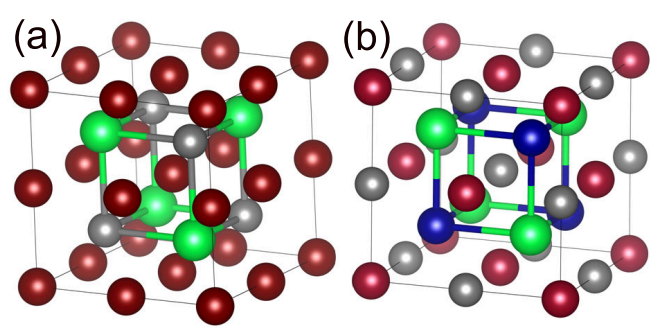

FIG. 1. (Color online) (a) The fcc $L2_1$ usual Heusler structure of Mn_2NiX (Ni_2MnX) systems. The red, gray and green spheres represents Mn (Ni), Ni (Mn) and X (X) atoms, respectively. (b) The fcc Hg_2CuTi inverse Heusler structure of Mn_2NiX systems. The red, blue, gray and green spheres represent MnI, MnII, Ni and X atoms, respectively.

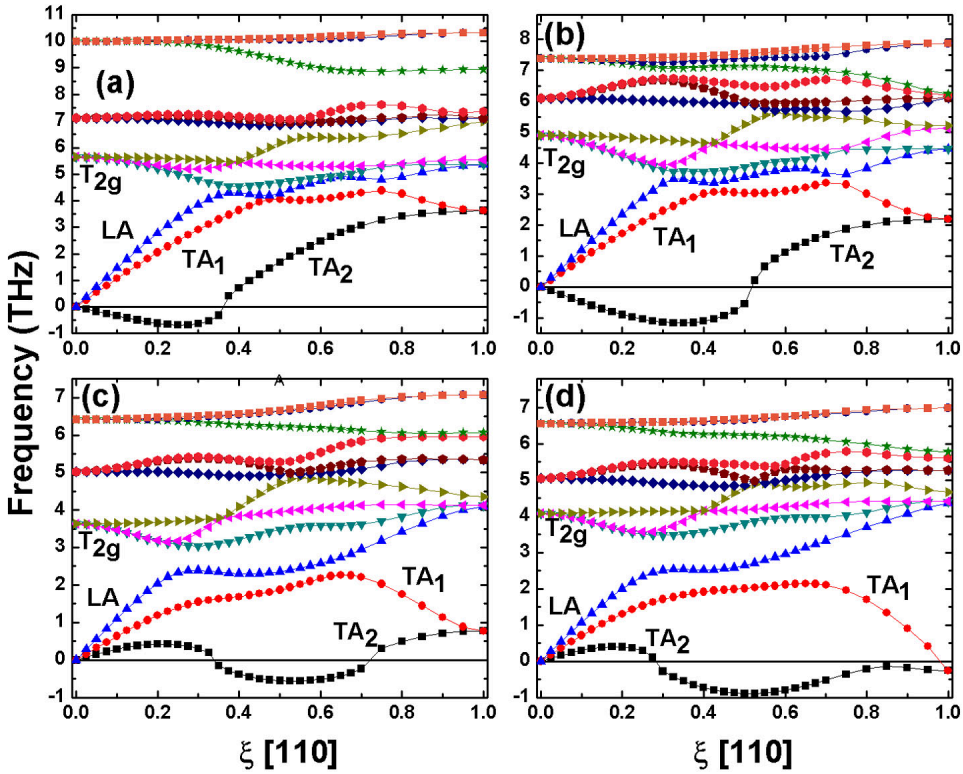

FIG. 2. (Color online) Phonon dispersion relations of (a) Mn_2NiAl, (b) Mn_2NiGa, (c) Mn_2NiIn and (d) Mn_2NiSn along [$\xi\xi$0] highly symmetric direction of the Brillouin zone. The phonon wave vector ξ is expressed in units of ($\frac{2\pi}{a}$).

Experimental measurements[14–16,29]and theoretical calculations[19–22]have confirmed that the alloys considered here favor Hg_2CuTi structure (Space group $F\bar{4}3m$), also known as inverse Heusler structure, in the cubic austenite phase as opposed to the usual Heusler structure of Ni_2MnX. The latter structure is best visualized as four interpenetrating f.c.c sub-lattices at (0,0,0), (0.25,0.25,0.25), (0.50,0.50,0.50) and (0.75,0.75,0.75), where the first and the third positions are occupied by Mn atoms, second and the fourth positions by Ni and X atoms, respectively(FIG. 1(a)). Interchanging the tetrahedral Mn atom at (0.50,0.50,0.50) with octahedral Ni atom at (0.25,0.25,0.25) keeping the remaining atoms fixed at their positions, leads to inverse Heusler structure (FIG. 1(b)). Hereafter, Mn atom at (000) sub-lattice will be denoted as MnI and the one at (0.25,0.25,0.25) as MnII.

Due to the unavailability of experimental results on the lattice constants of Mn_2NiAl and Mn_2NiIn, we have calculated the equilibrium lattice constants of all the four materials with GGA exchange-correlation functional and used them here. The total energies as a function of lattice parameters were fitted to Murnaghan equation of state to accurately calculate the equilibrium lattice constants. Our calculated lattice constant for Mn_2NiGa is 5.85 Å and for Mn_2NiSn is 6.15 Å which agree well with the available experimental results, i.e., 5.90 Å for Mn_2NiGa[15] and 6.1 Å for Mn_2NiSn[29]. On the other hand, our calculated lattice constants for Mn_2NiIn (a= 6.16 Å) matches well with available theoretical result[21]. Since the experimental results, for Mn_2NiGa and Mn_2NiSn, agree well with our calculated results, we consider our lattice constants as good representations of the experimental ones. The phonon dispersion spectra calculated at those lattice constants along [$\xi\xi$0] highly symmetric direction in the irreducible segment of the Brillouin zone (IBZ) are shown in FIG. 2. The main interest lies in the transverse acoustic TA_2 branch, which exists due to the atomic displacements [$\xi\bar{\xi}$0] perpendicular to the propagation direction [$\xi\xi$0]. For all Heusler systems exhibiting martensitic transformation, this branch shows an anomalous behavior. Therefore, our aim is to investigate the behavior of acoustic TA_2 branch along [$\xi\xi$0] direction. The most important features in the dispersion curves are the anomalous dips of the acoustic TA_2 branches where the phonon frequencies become imaginary, suggesting instabilities in the cubic austenite structures which usher in a phase transition to stable martensitic phases in all four materials. In Mn_2NiGa and Mn_2NiAl, the acoustic TA_2 branches have negative slopes at Γ point, indicating a pure elastic instability in their parent structure. The range of this instability extends up to ξ=0.50 for Mn_2NiGa and up to ξ=0.35 for Mn_2NiAl. The maximum of the dip occur at wave vectors ξ=0.35 and ξ=0.25 for Mn_2NiGa and Mn_2NiAl, respectively. For Mn_2NiIn, the instability of TA_2 branch starts from ξ=0.3 produc-

ing maximum of the dip at wave vector ξ=0.50. For Mn_2NiSn, unlike the other materials, the softening extends up to the wedge of the Brillouin zone with the maximum of the dip at ξ=0.50.

In previous studies of lattice dynamics on ternary MSMAs with Heusler structures, phonon anomalies of TA_2 were correlated with the precursor phenomenon prior to the martensitic phase when the systems are cooled from high temperatures. The wave vectors corresponding to the imaginary phonon frequencies indicated shuffling of atomic planes which stabilize the (c/a)<1 phases compared to the parent phase ((c/a)=1). The occurrence of 3M, 5M and 7M modulated structures and even incommensurate structures were confirmed experimentally. Possibilities of such modulated structures can be inferred from the anomalies in our calculated dispersion relations for Mn_2NiX systems. A modulated structure with a periodicity of 8 atomic planes (2M structure) can be associated with an instability at ξ=0.25, one with a periodicity of 6 atomic planes (3M structure) can be associated with an instability at ξ=0.33 and one with a shuffling of 14 atomic planes (7M structure) can be associated with an instability at ξ=0.29. For Mn_2NiAl, the unstable mode occurs for ξ=0.0 to ξ=0.35 with the maximum of the dip at ξ=0.25 . This suggests the possibilities of occurrence of several modulated phases. The commensurate wave vector closest to the maximum of the dip in the TA_2 branch of of Mn_2NiGa occurs at ξ=0.33 which can be related to the occurrence of the 3M structure. Since, in Mn_2NiGa, the imaginary frequencies extends up to ξ=0.50, in addition to aforementioned modulated structures 5M, modulation can also be observed at ξ=0.43 which stabilizes with the shuffling of 10 atomic planes. In cases of Mn_2NiIn and Mn_2NiSn, the maximum in the dip of the TA_2 branch occurs at ξ=0.5, which although cannot be connected to the known modulated structures mentioned above, but the extent of the instabilities in these systems can be connected to the 3M and 5M modulations. These suggest possibilities of occurrence of new kinds of modulations leading to precursor phenomena in these materials or that there may be more complicated structures with co-existence of multiple modulated phases. Signatures of 7M modulated phases have been observed experimentally[16,17] in Mn_2NiGa, but the occurrences of these were either dependent on the amount of stress in the system[17] or on the sublattice occupancies[16]. Thus, no definite conclusion on the kind of modulation in this system and the resulting pre-martensitic structures can be made from the available experimental results. Detailed systematic calculations on the non-cubic variants for these systems are to be carried out in order to settle the issue. However, this is beyond the aim and scope of the present study.

Energetically lowest optical T_{2g} branch is Raman active in nature with $[\xi\bar{\xi}0]$ polarization and the other optical branches are infrared active with T_1u symmetry. It is known that phonon branches with same symmetry would repel each other. Since, acoustic TA_2 branch also has same state of polarization; it would be repelled by the T_{2g} branches. In a previous theoretical study, Zayak *et al.*[30] argued that due to this repulsion the TA_2 branch is pushed downward and becomes unstable. To prove this, they compared the position of T_{2g} branches at Γ point of some stable Heusler alloys at cubic phase like Co_2MnGa and Co_2MnGe to unstable systems like Ni_2MnX (X =Ga, Ge, In, Al) and illustrated that energetically lowered T_{2g} branches in the unstable alloys compared to those alloys with stable cubic phases, produce the necessary repulsive thrust to the lowest vibrational branch. The results in FIG. 2 suggest the same explanation for the phonon instabilities in Mn_2NiX. The repulsion due to the already low lying T_{2g} modes at the Γ point for all four materials push the TA_2 frequencies down setting up the unstable modes. In reference 30, the authors attributed the occurrence of anomalous unstable modes in Ni_2MnGa to the inversion of modes of Ni and Ga. They showed that the contributions to the T_{2g} branches come from the dynamics of Ni atoms and due to the inversion of optical modes, the Ni atoms vibrate at lower frequencies making the frequencies of the T_{2g} mode lower. The repulsion of TA_2 modes by these T_{2g} modes pull the frequencies of the former down making them imaginary. For the materials investigated here, an analysis of the vibrational amplitudes show that the T_{2g} modes are dominated by the vibrations from Ni and MnI atoms who occupy crystallographic equivalent sites, and in fact the same ones as the two equivalent Ni atoms in Ni_2MnGa. Therefore, it would be interesting to examine whether such an inversion of optical mode is also happening for these materials. In the next subsection, we explore this by looking at the vibrational density of states (VDOS).

B. Vibrational density of states (VDOS)

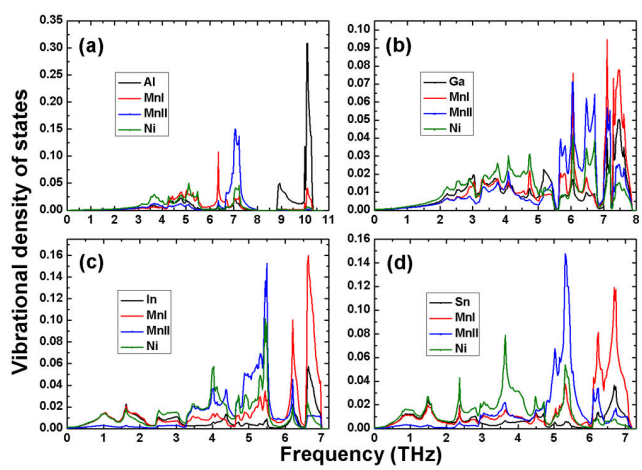

FIG. 3. (Color online) Atom projected vibrational density of states (VDOS) showing contributions from different constituent atoms for (a) Mn_2NiAl, (b) Mn_2NiGa, (c) Mn_2NiIn and (d) Mn_2NiSn over the frequency range.

In what follows, the atom projected VDOS for Mn_2NiAl, Mn_2NiGa, Mn_2NiIn and Mn_2NiSn are presented in FIG. 3. It is observed that the vibrational contributions from two Mn atoms occupy different frequency regions in the VDOS plots. This occurs mainly because of the following reasons: the two Mn atoms have different crystallographic symmetry; the atom occupying (000) sub-lattice, labeled as MnI, have tetrahedral symmetry and the other one at (0.25,0.25,0.25), labeled as MnII, sub-lattice have octahedral symmetry; as a consequence of this their nearest neighbor environments are different leading to different bond stiffness's (force constants) for the bonds connected to the Mn atoms. A comparison of all the VDOSs show that the VDOSs of Mn_2NiIn and Mn_2NiSn materials are quite similar and are very different from the VDOSs of the other two materials in the series. FIG. 3 suggests that for Mn_2NiIn and Mn_2NiSn, vibrations of MnI atoms are prominent between 6 THz to 7 THz, whereas contributions from MnII atoms are predominantly lie between 4.5 THz to 6 THz. Due to the slightly larger atomic mass than Mn atom, Ni vibrations occur mostly between 2.5 THz to 4.5 THz. As expected, the lower frequency regions are dominated by In and Sn because they have larger atomic masses than Ni and Mn. For Mn_2NiGa, vibrations in the range 7 THz to 8 THz are mainly dominated by MnI atom, while vibrations from 5.5 THz to 7 THz have contributions from MnII atoms. A strong peak originated from MnI vibrations coinciding with a peak originating from vibrations of MnII atoms is also observed at 6 THz. In the frequency range 3 THz to 5 THz, vibrations of Ni atoms are predominant and the lowermost part of the spectrum is dominated by the vibrations of the Ga atoms. The features in the VDOS of Mn_2NiAl is different than the other three. The modes due to the vibrations of Al atoms occur at around 10 THz due to extremely light mass of Al. The Ni modes also occur at lower frequencies, similar to the cases of the other three. The vibrations of MnI and MnII atoms dominate the middle of the spectrum with their respective peaks at 6.25 THz and 7.3 THz. In case of Ni_2MnGa, Zayak *et al.*[30] showed that the positions of Ga and Ni contributions to the VDOS were "inverted", that is, the vibrations of the lighter Ni atoms were at frequencies lower than those of heavier Ga atoms. They connected this anomalous mode inversion to the instability of the TA_2 modes of Ni_2MnGa. In case of the systems studied here, the overall features in the VDOSs of all four materials suggest that there is no signature of inversion of Ni (MnI) modes with those of the modes from the element X. Thus the occurrence of unstable TA_2 modes cannot be associated to this.

C. Inter-atomic force constants

In order to understand the features in the VDOS, we analyze the behavior of the real space inter-atomic force constants. In FIG. 4, we plot the longitudinal component of nearest neighbor force constants of Mn_2NiX systems. The transverse components of force constants are not shown in the plot, since, their contributions compared to the longitudinal ones are negligible. The force constants between any pair of nearest neighbor atoms are nearly equal for Mn_2NiAl with Mn_2NiGa. Same is true for Mn_2NiIn with Mn_2NiSn. However, substantial changes in the force constants between any pairs are observed as one moves from Mn_2NiGa to Mn_2NiIn. Due to the increase in the inter-atomic distances, as a result of expansion in their equilibrium lattice constants from 5.850 Å to 6.162 Å the MnI-MnII and MnII-Ni longitudinal force constants become softer in Mn_2NiIn and Mn_2NiSn in comparison to Mn_2NiGa. On the other hand, the force constants related to X elements, i.e., MnI-X and Ni-X become harder in Mn_2NiIn and Mn_2NiSn as compared to Mn_2NiGa and Mn_2NiAl. This opposite behavior is observed since the sizes of the X elements for the former two alloys are larger than those in the latter two, and thus are able to overcome the expansion of the inter-atomic distances occurring in the former two as compared to the latter two. The nearest neighbor force constants associated to MnII atom, the MnII-Ni and the MnII-MnI, become softer as one moves from Mn_2NiGa to Mn_2NiIn and Mn_2NiSn. Therefore, vibration frequencies corresponding to MnII atoms would be lower in the latter two materials, which agree with the features in the VDOS. In Mn_2NiGa, vibrations of MnII extend from 5.5 THz to 7 THz, which in case of Mn_2NiIn and Mn_2NiSn shift to lower frequencies, around 5.5 THz. The dynamical behavior of MnI and Ni atoms are more complicated. For both of the atoms, two sets of inter-atomic force constants behave opposite to one another. For Ni, the Ni-X nearest neighbor force constants harden, as one goes from Ga to In and Sn. This should force Ni atoms to

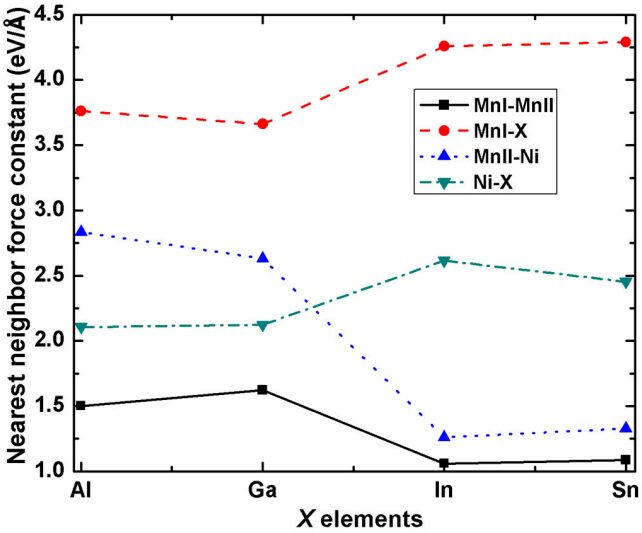

FIG. 4. (Color online) Longitudinal component of nearest neighbor inter-atomic force constants between MnI, MnII, Ni and X atoms of Mn_2NiX materials.

vibrate at higher frequencies as one goes from Mn_2NiGa to Mn_2NiIn and Mn_2NiSn. However, the vibrations of Ni atom remain more or less around the same frequency for all the materials, since the previous effect is compensated by increasing softening of the MnII-Ni bonds as one goes from Mn_2NiGa to Mn_2NiIn and Mn_2NiSn. Similarly, hardening of MnI-X force constant does not affect MnI vibrations, as this is compensated by the softening of MnI-MnII inter-atomic force constants.

D. Fermi surfaces

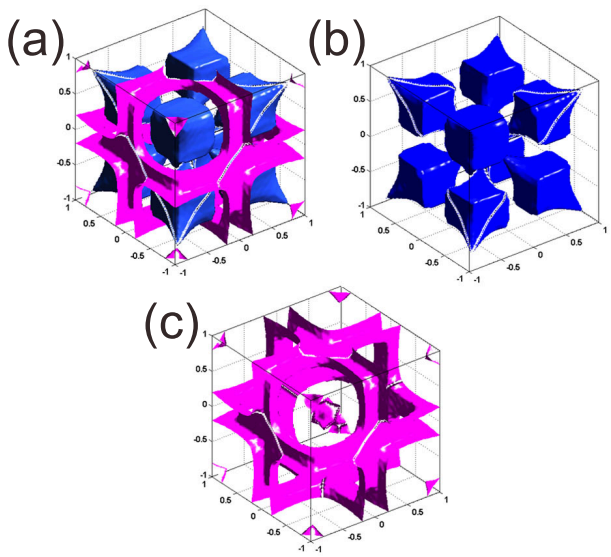

FIG. 5. (Color online) (a) Topology of 3D Fermi surfaces for Mn_2NiGa. The blue and magenta surfaces represent 18th and 19th spin minority bands, respectively. (b) and (c) illustrate those spin minority 18th and 19th bands separately.

Previous first-principles studies in Ni_2MnX relate the martensitic instability of those materials with Fermi surface nesting[30–34]. The anomalies in the phonon branch mainly depend on the shape of the Fermi surfaces and the electron-phonon matrix elements via the phonon wave vector ξ[32,33]. This phenomenon occurs due to strong attraction between two flat-parallel Fermi surfaces connected by a nesting vector **q**, at the expense of atomic displacements and at the wave vector where the maximum dip of the acoustic phonon branch is observed. However, this cannot be generalized for all ternary alloys showing martensitic instabilities. For Co_2NiGa, a newly found shape memory alloy, Siewart *et al.*[35] observed that softening in TA_2 phonon branch was absent as a result of nonappearance of nesting features in the Fermi surfaces of Co_2NiGa. Here, we present Fermi surfaces corresponding to the spin-minority bands only, since most prominent features are observed in this spin channel as the systems undergo martensitic transitions[19]. The three dimensional Fermi surfaces of Mn_2NiGa for

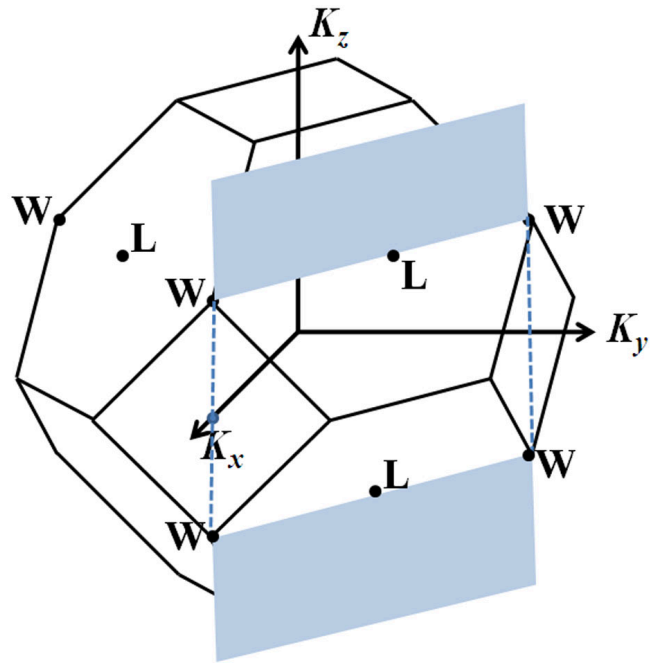

FIG. 6. (Color online) Illustration of the 110 cross section (k_x+k_y=1) in fcc irreducible Brillouin zone (IBZ).

18th and 19th spin-minority bands are shown in FIG. 5. The figure clearly exhibits flat portions of both the minority bands. However, to examine the Fermi surfaces in details, to obtain clues about the nesting between different parallel Fermi surfaces and hence, to relate this novel feature to observed phonon anomaly, two dimensional (2D) projections are necessary. In FIG. 7 we show the two-dimensional cross-sections of Fermi surfaces with the (110) plane for the four systems (The relevant portion of the Irreducible Brillouin zone is shown in FIG. 6). The cross-sections for Mn_2NiGa, Mn_2NiAl and Mn_2NiSn bear close resemblances while that of the Mn_2NiSn is somewhat different. Inspite of this difference, the nesting vectors (indicated by red arrows in Fermi surfaces plots) are consistent with the wave vectors at which the phonon anomalies are observed in our phonon dispersion curves. Thus, we can conclusively associate the occurrences of unstable modes in the Mn_2NiX alloys with the Fermi surface nesting. We refrain from further discussions on the differences in shapes of Fermi surfaces between materials with the element X belonging to different columns in the periodic table because it is not necessary in the present discussion where the focus is on to establish the nesting features in the Fermi surfaces and their relations to the martensitic instabilities found in these systems.

In reference 36, Barman *et al.* also computed the Fermi surfaces of Mn_2NiGa. Surprisingly, they observed Fermi surface nesting in the austenite phases along (100) and (010) directions only, and not along (110) direction like we did. The q value for one of the nesting vectors found by them is quite close to ours (The q value found by them is 0.31 which is very close to our value, q=0.35) though.

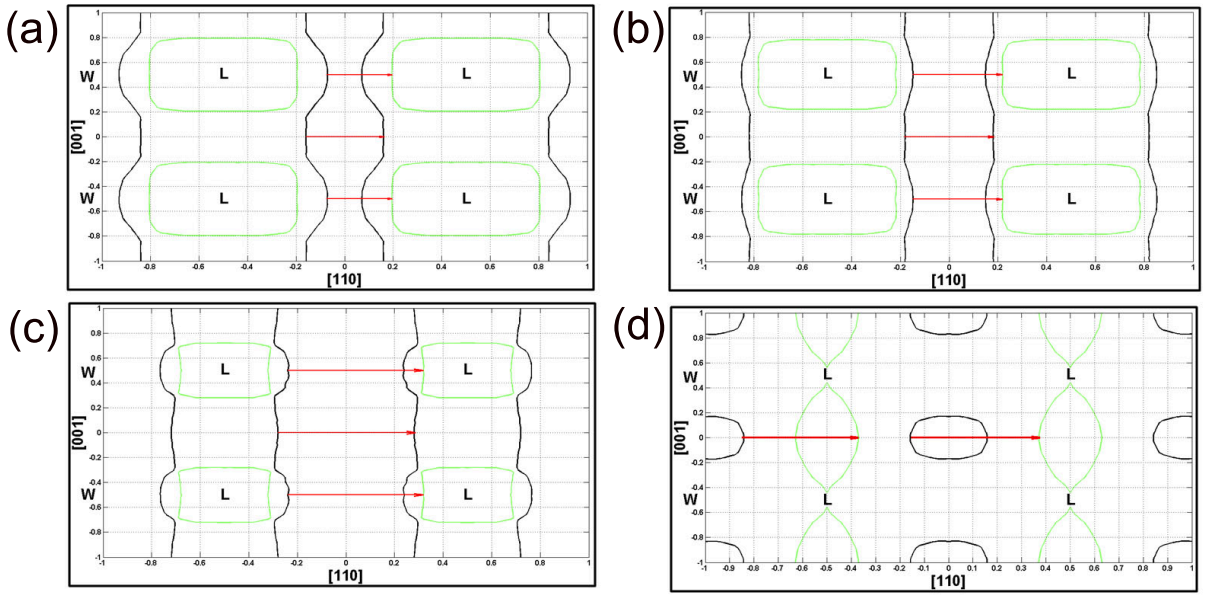

FIG. 7. (Color online) 2D cross section of the Fermi surfaces with the (110) plane k_x+k_y=1 for (a) Mn_2NiAl, (b) Mn_2NiGa, (c) Mn_2NiIn and (d) Mn_2NiSn. The green and black lines indicate spin minority bands. The red arrows indicate nesting vectors **q**=0.25(110) for Mn_2NiAl, **q**=0.35(110) for Mn_2NiGa and **q**=0.50(110) for Mn_2NiIn and Mn_2NiSn.

The nesting along (110) direction was observed by them in the martensitic phase with the q value 0.75. Though they attributed this to the possible instabilities in the TA_2 phonon mode, it wasn't substantiated by computations of the phonon spectra. Our results are qualitatively different from theirs as we found nesting along (110) direction in the austenite phase of Mn_2NiGa. Moreover, our results are consistent as the Fermi surface nesting along (110) could be related to the computed instabilities in the TA_2 phonon mode along (110) with the nesting vector computed from the Fermi surfaces agreeing with the wave vector at which the maximum of the instability occurs.

E. Elastic constants

TABLE I. Calculated elastic constants and elastic anisotropy ratio for Mn_2NiX materials. Experimental elastic constants are only available for Mn_2NiGa and shown in brackets.

Systems	c′ (GPa)	c_{11} (GPa)	c_{12} (GPa)	c_{44} (GPa)	A (=c_{44}/c')
Mn_2NiAl	-33.13	100.35	127.19	131.66	-3.97
Mn_2NiGa	-13.42	58.91 (90.55)[37]	125.17 (128.00)[37]	111.00 (124.42)[37]	-8.27
Mn_2NiIn	16.44	118.64	85.76	41.47	2.52
Mn_2NiSn	15.43	146.05	115.19	64.27	4.17

The dynamical stability of crystalline phase implies that the strain energy changes be positive definite against all possible small deformations. This condition imposes restrictions on elastic constants. The stability criteria for cubic crystals requires[38]

$$c_{44} > 0, c_{11} > |c_{12}|, c_{11} + 2c_{12} > 0 \quad (1)$$

Therefore to introspect the kinds of instabilities present in the materials considered here and to validate our calculated phonon dispersion results, we compute the elastic constants for all the four materials from the initial slope ($\xi \rightarrow 0$) of phonon dispersion plots along [$\xi\xi$0] direction. The elastic constants c_{44}, c′ ($=\frac{1}{2}(c_{11} - c_{12})$) and c_L ($=\frac{1}{2}(c_{11} + c_{12} + 2c_{44})$) are related to TA_1, TA_2 and LA acoustic modes[38]. These elastic constants are connected to ultrasound velocity via $c_{ij}=\rho v^2$ relation[38] where ρ is the mass density. The three independent elastic constants of cubic crystal are tabulated in TABLE I. Our computed c_{12} and c_{44} agree quite well with the experimental results available only for Mn_2NiGa, whereas in our calculation, c_{11} is underestimated[37]. Overall the agreement with experiment is good for Mn_2NiGa. This, in effect, is an indirect indication to the accuracy of calculated phonon spectra. The results show that the Equation (1) is satisfied by Mn_2NiIn and Mn_2NiSn only. This indicates that Mn_2NiAl and Mn_2NiGa are unstable in the cubic structure. We gain further insight into the nature of stabilities of these materials by looking at the other two parameters listed in TABLE I, the shear constant and the elastic anisotropy ratio. Since acoustic TA_2 branch is related to shear constant (c′), hence, negative c′ for Mn_2NiAl and Mn_2NiGa is an indication of pure elastic instability which stabilizes though shear deformation across ($\xi\xi$0) planes in [$\xi\bar{\xi}$0] direction. The same is not true for

the other two materials. Although they satisfy Equation (1) and have sizable c′, their anisotropy ratios A are high enough to bring in a martensitic transformation[39]. The elastic anisotropy ratio A (=c_{44}/c') is an important quantity to measure of stability of cubic structures under stress across ($\xi\xi0$) planes[40]. Larger the value it acquires, more unstable the structure becomes. For systems undergoing martensitic transformations, the value of A varies from 2 onward[11,39,41–44]. In cases of Mn_2NiIn and Mn_2NiSn, the values of A lie well within the limits observed in shape memory alloys. The origin of this could be rather small value of the shear modulus c′. Additionally, we find that c_{44} in cases of Mn_2NiIn and Mn_2NiSn are much softer than those for the other two materials. The comparative softening in c_{44} for Mn_2NiIn and Mn_2NiSn as compared to Mn_2NiGa and Mn_2NiAl, indicate that the cubic Mn_2NiIn and Mn_2NiSn will transform to different martensitic phases compared to the other two where the transformations would be driven by softening in c′ as has been observed in cases of other shape memory alloys[39]. The results on elastic constants therefore corroborate the inferences drawn from the differences in dispersion relations for the materials studied.

The vibrational and elastic properties discussed in this work show a clear trend. Mn_2NiGa and Mn_2NiAl are quite similar in their behaviors; same goes for Mn_2NiIn and Mn_2NiSn. The vibrational and elastic properties among these two groups are significantly different. The origin of such differences can be traced back to the differences in their electronic structures[19]. The signatures of mechanical instability were reflected in electronic structures of Mn_2NiGa and Mn_2NiAl, where high densities of states, as compared to Mn_2NiIn and Mn_2NiSn, were found at the Fermi level. The origin of this was larger hybridizations between the Mn and Ni atoms at the octahedral positions for the former two systems. For the latter two systems, rather small densities of states at Fermi level, due to smaller hybridizations between the magnetic atoms at octahedral positions, originating from larger distances between those magnetic atoms (due to the atoms sitting in a larger lattice compared to the former two which happens as In and Sn have larger sizes than Ga and Al), signified that it would take external influences to induce instabilities into these systems.

IV. SUMMARY AND CONCLUSIONS

We have investigated the lattice dynamics of Mn_2NiX (X= Al, Ga, In, Sn) MSMAs in their austenite phase using first-principles based density functional theory calculations. The calculated phonon spectra show anomalous behavior of the acoustic TA_2 branch along [$\xi\xi0$] direction for all the four materials indicating structural instability. Instabilities in the said acoustic mode can be related to the repulsion by the optical T_{2g} mode having the same symmetry as the TA_2 mode. Unlike Ni_2MnGa, no inversion of optical modes could be observed, thus ruling this out as one of the possible mechanisms behind the anomalous features in phonon spectra. The features in the vibrational densities of states can be explained from the qualitative variations of the interatomic force constants across the materials. The calculated elastic constants corroborate the structural instabilities inferred from phonon dispersion relations. Negative shear constants for Mn_2NiAl and Mn_2NiGa indicate pure elastic instabilities in these materials. Finally, the nesting features in the Fermi surfaces confirm that the observed phonon anomalies are associated with them. The wave vectors at which the maximum anomaly occur indicate the possibility of formation of pre-martensitic modulated phases which are yet to be confirmed by experiments. The results also indicate that these modulated pre-martensitic phases could be quite complex and further investigations into this aspect is necessary.

V. ACKNOWLEDGMENTS

Financial assistance from the Swedish Research Links (VR-SIDA) is acknowledged. The Swedish National Computing facilities, computation facilities from C-DAC, Pune, India and from Department of Physics, IIT Guwahati funded under the FIST programme of DST, India are also acknowledged. SG and SP would like to acknowledge Dr. Munima B. Sahariah, IASST, Guwahati, India for the help in plotting the Fermi surfaces.

* For correspondence: subhra@iitg.ernet.in

[1] K. Ullakko, J. K. Huang, C. Kanter, R. C. O'Handley and V. V. Kokorin, *Appl. Phys. Lett.* **69**, 1966 (1996).
[2] A. Sozinov, A. A. Likhachev, N. Lanska and K. Ullakko, *Appl. Phys. Lett.* **80**, 1746 (2002).
[3] A. Zheludev, S. M. Shapiro, P. Wochner, A. Schwartz, M. Wall and L. E. Tanner, *Phys. Rev. B* **51**, 11310 (1995).
[4] A. Zheludev, S. M. Shapiro, P. Wochner and L. E. Tanner, *Phys. Rev. B* **54**, 15045 (1996).
[5] L. Mañosa, A. Planes, J. Zarestky, T. Lograsso, D. L. Schlagel and C. Stassis, *Phys. Rev. B* **64**, 024305 (2001).
[6] A. T. Zayak, P. Entel, J. Enkovaara, A. Ayuela and R. M. Nieminen, *Phys. Rev. B* **68**, 132402 (2003).
[7] A. T. Zayak and P. Entel, *J. Magn. Magn. Mater.* **290-291**, 874 (2005).
[8] X. Moya, L. Mañosa, A. Planes, T. Krenke, M. Acet, V. O. Garlea, T. A. Lograsso, D. L. Schlagel and J. L. Zarestky, *Phys. Rev. B* **73**, 064303 (2006).
[9] T. Büsgen, J. Feydt, R. Hassdorf, S. Thienhaus, M. Moske, M. Boese, A. Zayak and P. Entel, *Phys. Rev. B* **70** 014111 (2004).
[10] S. Ağduk and G. Gökoğlu, *Eur. Phys. J. B* **79**, 509 (2011).

[11] S. Ağduk and G. Gökoğlu, *J. Alloys Compd.* **511**, 9 (2012).
[12] P. J. Webster, K. R. A. Ziebeck, S. L. Town and M. S. Peak, *Philo. Mag. B* **49**, 295 (1984).
[13] A. Zheludev, S. M. Shapiro and P. Wochner, *Phys. Rev. B* **54**, 15045 (1996).
[14] G. D. Liu, J. L. Chen, Z. H. Liu, X. F. Dai, G. H. Wu, B. Zhang and X. X. Zhang, *Appl. Phys. Lett.* **87**, 262504 (2005).
[15] G. D. Liu, X. F. Dai, S. Y. Yu, Z. Y. Zhu, J. L. Chen, G. H. Wu, B. Zhang and X. X. Zhang, *Phys. Rev. B* **74**, 054435 (2006).
[16] S. Singh, M. Maniraj, S. W. D'Souza, R. Ranjan and S. R. Barman, *Appl. Phys. Lett.* **96**, 081904 (2010).
[17] P. J. Brown, T. Kanomata, K. Neumann, K. -U. Neumann, B. Ouladiaff, A. Sheikh and K. R. A. Ziebeck, *J. Phys.: Condens. Matter.* **22**, 506001 (2010).
[18] N. Lakshmi, K. Pandey and N. Venugopalan, *Bull. Mater. Sci.* **25**, 309 (2002).
[19] S. Paul and S. Ghosh, *J. Appl. Phys.* **110**, 063523 (2011).
[20] S. R. Barman and A. Chakrabarti, *Phys. Rev. B* **77**, 176401 (2008).
[21] A. Chakrabarti and S. R. Barman, *Appl. Phys. Lett.* **94**, 161908 (2009).
[22] H. Luo, G. Liu, F. Meng, S. Li, W. Zhu, G. Wu, X. Zhu and C. Jiang, *Physica B* **405**, 3092 (2010).
[23] S. Paul, B. Sanyal and S. Ghosh, *J. Phys.: Condens. Matter.* **25**, 236005 (2013).
[24] P. Giannozzi, S. Baroni, N. Bonini, M. Calandra, R. Car, C. Cavazzoni, D. Ceresoli, G. L. Chiarotti, M. Cococcioni, I. Dabo, A. Dal Corso, S. de Gironcoli, S. Fabris, G. Fratesi, R. Gebauer, U. Gerstmann, C. Gougoussis, A. Kokalj, M. Lazzeri, L. MartinSamos, N. Marzari, F. Mauri, R. Mazzarello, S. Paolini, A. Pasquarello, L. Paulatto, C. Sbraccia, S. Scandolo, G. Sclauzero, A. P. Seitsonen, A. Smogunov, P. Umari and R. M. Wentzcovitch, *J. Phys.: Condens. Matter.* **21**, 395502 (2009).
[25] D. Vanderbilt, *Phys. Rev. B* **41**, 7892 (1990).
[26] J. P. Perdew in *Electronic Structure of Solids*, edited by P. Ziesche and H. eschrig, (Akademic Verlag, Berlin 1991), p. 11.
[27] M. Methfessel and A. T. Paxton, *Phys. Rev. B* **40**, 3616 (1989).
[28] S. Baroni, S. De Gironcoli, A. Dal Corso and P. Giannozzi, *Rev. Mod. Phys.* **73**, 515 (2001).
[29] R. B. Helmholdt and K. H. J. Buschow, *J. Less-Comm. Metals* **128**, 167 (1987).
[30] A. T. Zayak, P. Entel, K. M. Rabe, W. A. Adeagbo and M. Acet, *Phys. Rev. B* **72**, 054113 (2005).
[31] Y. Lee, J. Y. Rhee and B. N. Harmon, *Phys. Rev. B* **66**, 054424 (2002).
[32] C. Bungaro, K. M. Rabe and A. Dal Corso, *Phys. Rev. B* **68**, 134104 (2003).
[33] O. I. Velikokhatnyi and I. I. Naumov, *Phys. Solid State* **41**, 617 (1999).
[34] P. Entel, V. D. Buchelnikov, M. E. Gruner, A. Hucht, V. V. Khovailo, S. K. Nayak and A. T. Zayak, *Mater. Sci. Forum* **583**, 21 (2008).
[35] M. Siewert, M. E. Gruner, A. Dannenberg, A. Hucht, S. M. Shapiro, G. Xu, D. L. Schlagel, T. A. Lograsso and P. Entel, *Phys. Rev. B* **82**, 064420 (2010).
[36] S. R. Barman, S. Banik, A. K. Shukla, C. Kamal and A. Chakrabarti, *Europhys. Lett.* **80**, 57002 (2007).
[37] Z. Jian-Tao, Z. Kun, W. Jia-Jia, Y. Xin-Quan, Y. Jin and W. San-Xie, *Acta. Phys. Sin.* **61** 213102 (2012).
[38] M. Born and K. Huang, in *Dynamical Theory of Crystal Lattices*, (Clarendon, Oxford, 1956).
[39] K. Otsuka and X. Ren, in *Progress in Materials Science*, **50**, 511 (2005).
[40] C. M. Zener, *Phys. Rev.* **71**, 846 (1947).
[41] T. Černoch, M. Landa, P. Novák, P. Sedlák and P. Šittner, *J. Alloys. compd.* **378**, 140 (2004).
[42] S. M. Shapiro, G. Xu, G. Gu, J. Gardner and R. W. Fonda, *Phys. Rev. B* **73**, 214114 (2006).
[43] S. M. Shapiro, G. Xu, B. L. Winn, D. L. Schlagel, T. Lograsso and R. Erwin, *Phys. Rev. B* **76**, 054305 (2007).
[44] A. Planes and L. Mañosa, *Solid State Phys.* **55**, 159 (2001).